CONDENSED MATTER

Thermo-Elastic and Lattice Dynamical Properties of Pd$_3$X (X=Ti, Zr, Hf) Alloys: An Ab Initio Study

G. Surucu [1,2] · K. Colakoglu [2] · Y. O. Ciftci [2] · H. B. Ozisik [3] · E. Deligoz [3]

Abstract Using the generalized–gradient approximation (GGA) based on density functional theory, we have reported the structural, mechanical, electronic, and lattice dynamical properties of the intermetallic compounds Pd$_3$X (X=Ti, Zr, Hf) with D0$_{24}$ and the L1$_2$ structures. The elastic constants were predicted using the stress-finite strain technique. We performed numerical estimations of the bulk modulus, shear modulus, Young's modulus, Poisson's ratio anisotropy factor, G/B ratio, and hardness. Our studies have showed that all Pd$_3$X (X=Ti, Zr, Hf) with D0$_{24}$ and the L1$_2$ structures are mechanically stable and relatively hard materials with low compressibility, and they could be considered as ductile systems. Also, the phonon dispersion curves and total and partial density of states were calculated and discussed for Pd$_3$X (X=Ti, Zr, Hf). We finally estimated some thermodynamic properties such as entropy, free energy, and heat capacity at the temperature range 0–1000 K. The calculated phonon frequencies of Pd$_3$X (X=Ti, Zr, Hf) are positive, indicating the dynamical stability of the studied compounds. For the first time, we have performed the numerical estimation of lattice dynamical properties for the compounds and still awaits experimental confirmation. The obtained ground state properties are in good agreement with those of experimental and theoretical studies.

✉ E. Deligoz
edeligoz@yahoo.com

1   Kaman MYO, Ahi Evran University, Kaman, 40100 Kirsehir, Turkey

2   Department Of Physics, Teknikokullar, Gazi University,
     06500 Ankara, Turkey

3   Department Of Physics, Aksaray University, 68100 Aksaray, Turkey

1 Introduction

Palladium is the only one transition element with the (formal) completely filled d shell (4d^{10}) and shows exceptional strong metallic bonding [1]. Recent developments in material processing suggest that intermetallic may be useful in structural applications where ceramics are now contemplated for use [2]. Some important properties of these alloys can be improved by alloy addition, directional solidification, and through the use of single crystals [3, 4]. Pd-X (X=Ti, Zr, Hf) alloys have gained increasing attention in recent years due to their interesting mechanical properties and technological importance for engineering and medicine [5, 6], particularly the shape-memory effect [7–9], the property of reversible hydrogen storage [10, 11], and the improvement of corrosion resistance [12, 13].

The Pd-X (X=Ti, Zr, Hf) system belongs to a class of binary alloy system which combines so-called "early" and "late" transition elements. Previous studies on this class of alloys have revealed a variety of intriguing phenomena such as charge density waves [14–17], lattice displacement structure [17–24], martensitic transformations, and superconductivity. These phenomena are often associated with Fermi surface instabilities and can produce some unique and useful properties [25]. It was predicted by Brewer nearly 50 years ago [26] that the binary intermetallic compounds formed between early transition metals and late transition metals should be very stable. Almost all previous experimental determinations and theoretical estimations have in fact indicated large negative enthalpies of formation for such compounds [27],

which this quantity has been indicating an exceptional affinity between atoms of these transition metal components [28].

The unit cell parameters were measured experimentally for binary palladium- and platinum-rich alloys containing the A4 early transition metals (titanium, zirconium, and hafnium) by Ellner [28]. Pd$_3$Ti is known to exist in two stable forms: the hexagonal TiNi$_3$-type (hP16, D0$_{24}$) structure [29–31] and (with excess Pd) the cubic AuCu$_3$-type (cP4, L1$_2$) structure [32]. Also, the stability of Pd$_3$Zr–D0$_{24}$ with hexagonal Ni$_3$Ti-type and PdZr$_2$–C11$_b$ with a tetragonal MoSi$_2$-type was confirmed in [33]. The intermetallic compounds in the Pd–Hf binary system have the following structures: Pd$_3$Hf (hP16, TiNi$_3$-type), Pd$_2$Hf (tI6, MoSi$_2$ type), PdHf$_2$ (tI6, CuZr$_2$-type), and PdHf$_2$ (cF96, Ti$_2$Ni type) [34].

Theoretically, the effect of an alloying metal and its magnetic state on the hydrogen absorption energy was investigated in the Pd-based alloys Pd$_3$Me with 3d transition metals (Me=Ti, V, Cr, Mn, Fe, Co, Ni, and Cu) based on the first principles by Minibaev et al. [35]. Mikusik et al. calculated heats of formation for transition metal alloys MTi and M$_3$Ti (M=Ni, Pd, Pt) by self-consistent tight-binding method [36]. Electronic properties of the Pd$_3$Ti alloy and some related surface structures were studied within a simple charge self-consistent LCAO d-band model by Pick et al. [37]. The thermodynamic properties and phase diagram of the Pd-Zr system were analyzed by the CALPHAD technique using a computational optimization procedure by Gua et al. [38]. Experimentally, Gua et al. [39] determined the standard enthalpies of formation of ten alloys formed between group IV elements (Ti, Zr, Hf) and group VIII element (Rh, Pd, Pt) in the periodic table by high-temperature direct synthesis calorimetry at 1477±2 K.

The recent studies about Pd-Ti and Pd-Zr systems including Pd$_3$Ti and Pd$_3$Zr can be given as follows: Chen et al. investigated the ground state phase stabilities, enthalpies of formation, electronic and elastic properties of Ti-Pd alloy system, and associated hydrides using an ab initio density functional approach [40]. Experimentally, the standard enthalpies of formation of some late 4d and 5d transition metals including Pd$_3$Hf were measured by high temperature, direct synthesis calorimetry at 1373±2 K by Meschel et al. [41]. Theoretically, the thermodynamic properties of Pd-Ti system were optimized using CALPHAD (Calculation of Phase Diagram) technique from the experimental information available in the literature [41]. Their studies show that the intermetallic compounds Pd$_3$Ti, Pd$_3$Ti$_2$, and PdTi$_3$ are treated as stoichiometric compounds. Hu et al. [25] reported the electronic, elastic, and structural properties of Pd-Zr system by using first-principle calculations for only stable phases obtained experimentally. Finally, Bai et al. [42] investigated formation enthalpies, elastic constants, and bulk modulus of 133 phases for the Pd-Zr system including stable phase and hypothetical ones. Also in our previous work, we successfully predicted the

lattice dynamical and thermo-elastic properties of Rh$_3$X (X= Ti, V, Hf) compounds within DFT-PBE and PAW method [43, 44].

Predicting some fundamental material properties, i.e. the crystalline structures, formation enthalpies, bulk modulus, elastic constants, phonon frequencies, etc. have been well known to be a vital important issue for the physicists, chemists, and materials scientists. The purpose of this work is to provide some additional information to the existing data on the some physical properties of Pd$_3$X (X=Ti, Zr, Hf) using first-principle calculations. Especially, we focus on the mechanical, lattice dynamical, and temperature-dependent thermodynamical properties of Pd$_3$X (X=Ti, Zr, Hf) alloys.

2 Method of Calculation

In the present paper, first-principle calculations were carried out using the Vienna ab initio simulation package (VASP) [45–48] based on the density functional theory (DFT). The electron-ion interaction was considered in the form of the projector-augmented-wave (PAW) method with plane wave up to energy of 400 eV [47, 49]. For the exchange and correlation terms in the electron-electron interaction, Perdew-Burke-Ernzerhof (PBE) functional [50] was used within the generalized gradient approximation (GGA). The parameter that affects the accuracy of calculations is the kinetic energy cut-off, which determines the number of plane waves in the expansion and the number of special k-points used for the Brillouin zone (BZ) integration. We performed convergence tests with respect to BZ sampling and the size of the basis set. The converged results were achieved with $11 \times 11 \times 6$ and $10 \times 10 \times 10$ for D0$_{24}$ and L1$_2$ phases, respectively. The special k-point mesh were produced using the Monkhorst–Pack grid [51]. The energy tolerance was less than 10^{-8} eV per unit cell in the iterative solution of the Kohn–Sham equations. The structures were relaxed until the forces on each atom were less than 0.01 eV/Å.

3 Results and Discussion

3.1 Structural Properties

In this paper, we have considered hexagonal Ni$_3$Ti-type (D0$_{24}$, P6$_3$/mmc, Space Group No: 194) and cubic Cu$_3$Au (L1$_2$, Pm-3 m, Space Group No: 221) structures. To get fully relaxed structures of Pd$_3$X (X=Ti, Zr, Hf) compounds, both lattice geometry and ionic positions were fully optimized. Our results, in good agreement with corresponding the experimental [29–32, 53] and theoretical values [25, 40, 42], are tabulated in Table 1 together. But in the case of the calculated lattice parameters, there are an average deviation of about 0.9 and

Table 1 The calculated lattice constants (*a* and *c* in Å) and formation energies (ΔH_f in kJ/mole of atoms) for Pd₃X (X=Ti, Zr, Hf)

Material			a	c	ΔH_f
Pd₃Ti (D0₂₄)	Present	GGA	5.540	9.041	−64.80
	Theory [40]	GGA	5.555	9.063	−62.90
	Exp. [29]		5.489	8.964	
	Exp.[30]		5.489	8.614	
	Exp. [31]		5.489	8.964	
	Exp. [39]				−65.00
	Exp. [51]				−50.70
Pd₃Ti (L1₂)	Present	GGA	3.940		−62.43
	Theory [40]	GGA	3.926		
	Exp. [32]		3.820		
Pd₃Zr (D0₂₄)	Present	GGA	5.68	9.33	−80.83
	Exp. [39]				−84.40
	Exp. [52]				−82.80
	Theory [25]	GGA	5.636	9.275	−84.41
	Theory [42]	GGA	5.667	9.321	−80.80
	Exp. [53]		5.612	9.235	
Pd₃Zr (L1₂)	Present	GGA	4.03		−78.15
	Theory [42]	GGA	4.01		−78.20
Pd₃Hf (D0₂₄)	Present	GGA	5.64	9.27	−88.32
	Exp. [39]				−88.50
	Exp. [52]				−100.10
Pd₃Hf (L1₂)	Present	GGA	4.01		−85.87

1.2 % from the earlier experimental data [29–32, 39, 52, 54] for *a* and *c* in D0₂₄ structure of Pd₃X (X=Ti, Zr, Hf), respectively. These deviations may be attributed to the fact that the experimental sample was synthesized as thin film by vapor phase deposition [54] at 450 °C D0₂₄ structure for Pd-Ti system. This structure exists in the composition range of about

18–27 at.% of Zr at 1873 K, but this range narrows significantly at lower temperatures for Pd-Zr systems [53], whereas our calculations correspond to the perfect bulk materials at zero temperature. Also, some divergences are related to the well-known overestimation of lattice parameters within GGA-based calculation methods.

From total energy of the compound and constituent elemental solids, one can compute the formation energy using the following common relation:

$$E_{\text{form}}^{\text{Pd}_3\text{X}} = E_{\text{total}}^{\text{Pd}_3\text{X}} - \left[3E_{\text{solid}}^{\text{Pd}} + E_{\text{solid}}^{\text{X}} \right] \tag{1}$$

The calculated formation energies are also listed in Table 1. It is seen that all of the formation energies of Pd₃X (X = Ti, Zr, and Hf) are negative implying that all considered compounds can be synthesized more easily as a thermodynamically stable phase. The formation energy of the cubic L1₂-type structure is slightly higher than that of the D0₂₄-type structure, indicating the cubic L1₂-type structure of Pd₃X (X=Ti, Zr, Hf) could exist as a meta-stable phase as given in [40]. It can be seen from Table 1, among the considered compounds, Pd₃Hf is, relatively, the most stable one.

3.2 Mechanical Properties

The elastic constants C_{ij}, which contain more important information, can be obtained from ground state total energy calculations [55]. The elastic constants are related to some fundamental properties such as interatomic potential, equation of state, phonon spectra, specific heat, Debye temperature, and melting point. The elastic constants are calculated by using the stress-strain relations [56], and the results are given in Table 2. The traditional mechanical stability conditions in a cubic and hexagonal crystal systems on the elastic constants are {C_{11}−

Table 2 The calculated elastic constants (C_{ij} in GPa), bulk modulus (*B* in GPa), isotropic shear modulus (*G* in GPa), *G/B* rations, Young's modulus (*E* in GPa), and Poisson's ratio (*v*) for Pd₃X (X=Ti, Zr, Hf)

Material			C_{11}	C_{12}	C_{13}	C_{33}	C_{44}	B	G	G/B	E	v
Pd₃Ti (D0₂₄)	Present	(GGA)	317.7	123.3	114.6	321.2	73.6	184.9	88.2	0.48	228.2	0.29
	Theory [40]	(GGA)	306.4	124.6	112.7	317.8	71.0	181.2	80.3		209.9	0.31
	Theory [58]		331.1	110.3	65.5	334.8	66.4					
Pd₃Ti (L1₂)	Present	(GGA)	261.6	136.7			105.3	178.4	85.3	0.48	220.6	0.29
Pd₃Zr (D0₂₄)	Present	(GGA)	302.6	119.2	111.3	307.7	72.0	177.4	84.4	0.47	218.7	0.29
	Theory [42]	(GGA)	268	90	99	305	70					
	Theory [25]	(GGA)	334.2	139.1	157.9	390.6	75.5	218.8	89.1	0.41	235.2	
	Theory [58]		352.4	118.9	89.9	405.3	87.1					
Pd₃Zr (L1₂)	Present	(GGA)	219.9	145.4			89.1	170.3	62.8	0.37	167.1	0.33
Pd₃Hf (D0₂₄)	Present	(GGA)	317.3	126.6	117.2	321.6	74.0	186.4	87.5	0.47	227.0	0.30
	Theory [58]		341.5	113.4	74.8	365.1	75.8					
Pd₃Hf (L1₂)	Present	(GGA)	231.5	154.0			94.0	179.0	65.9	0.37	176.1	0.34

$C_{12}>0$, $C_{44}>0$, $C_{11}+2C_{12}>0$} and {$C_{11}-C_{12}>0$, $C_{11}+C_{12}+C_{33}>0$, $(C_{11}+C_{12})\,C_{33}>2C_{13}{}^2>0$, $C_{44}>0$}, respectively [43, 44, 57, 58]. Our results for elastic constants in Table 2 obey these stability conditions, hence we can say that Pd$_3$X (X=Ti, Zr, Hf) are mechanically stable in both D0$_{24}$ and L1$_2$ structures. As shown in Table 2, the calculated results are close to the each other and the values reported in [25, 40, 42, 58] for Pd$_3$X (X=Ti, Zr, Hf). It can be seen from Table 2 that unidirectional elastic constants C_{11} and C_{33} are about ~75 % higher than C_{44}. This indicates that these compounds present a weaker resistance to shear deformation compared to the resistance to the unidirectional compression.

Poisson's ratio (ν), Young's modulus (E), Bulk modulus, and shear modulus (G) are calculated in terms of the computed data using the following relations [59]:

$$\nu = \frac{1}{2}\left[\frac{\left(B-\frac{2}{3}G\right)}{\left(B+\frac{1}{3}G\right)}\right] \quad (2)$$

and

$$E = \frac{9GB}{G+3B} \quad (3)$$

where $B=(B_v+B_R)/2$ and $G=(G_v+G_R)/2$ are the isotropic shear modulus, G_V is Voigt's shear modulus corresponding to the upper bound of G values, and G_R is Reuss's shear modulus corresponding to the lower bound of G values, and can be written as $B_v=B_R=(C_{11}+2C_{12})/3$, $G_v=(C_{11}-C_{12}+3C_{44})/5$, and $5/G_R=4/(C_{11}-C_{12})+3/C_{44}$ for cubic phases, $B_v=(1/9)[2\,(C_{11}+C_{12})+4C_{13}+C_{33}]$ $G_v=(1/30)\,(M+12C_{44}+12C_{66})$, $M=C_{11}+2C_{33}-4C_{13}$, $B_R=C^2/M$, $C^2=(C_{11}+C_{12})C_{33}-2C_{13}{}^2$ $G_R=(5/2)\,\left(C^2C_{44}C_{66}\right)/\left[3B_vC_{44}C_{66}+C^2(C_{44}+C_{66})\right]$ for hexagonal phases.

Exploring the mechanical properties, the results obtained from our *ab initio* calculations for bulk modulus (B), Poisson ratio (ν), Young's modulus (E), and G/B rations of Pd$_3$X (X=Ti, Zr, Hf) are listed in Table 2.

As a fundamental physical property, the bulk moduli of solids also provide valuable information on the bond strength of atoms for a given crystal [60]. The bulk modulus is a measure of resistance to volume change by applied pressure, whereas the shear modulus is a measure of resistance to reversible deformations upon shear stress [61]. The bulk moduli (B) decrease in the sequence: B(Pd$_3$Hf)>B(Pd$_3$Ti)>B(Pd$_3$Zr). The highest value of bulk modulus (186.4 GPa) is obtained for D0$_{24}$ structure of Pd$_3$Hf. We have concluded that Pd$_3$Zr is the highest compressible one among the Pd$_3$X compounds because the low bulk modulus shows high compressible material. As the bulk modulus can be used as a measure of the average inter-atomic bond strength [61], this trend coincides with the weakening of bonding strength in Pd$_3$Zr. In general,

the obtained bulk modulus for D0$_{24}$ structure of Pd$_3$Ti and Pd$_3$Zr is in accordance with the theoretical results [25, 40]. Unfortunately, there is no experimental or theoretical data for comparing with the present results for cubic (L1$_2$) Pd$_3$X compounds.

It is known that shear modulus describes the resistance of a material to shape change. The calculated isotropic shear moduli are 88.2, 84.4, and 87.5 GPa for D0$_{24}$ structure and 85.3, 62.8, and 65.9 GPa for L1$_2$ structure of Pd$_3$X (X=Ti, Zr, Hf), respectively. Young's modulus is defined as the ratio of stress and strain and is used to provide a measure of stiffness of the solid. The material is stiffer if the value of Young's modulus is high. Therefore, these compounds are stiffer due to the higher value of Young's modulus. The values of Young's modulus for Pd$_3$Ti and Pd$_3$Hf are nearly same within standard numerical errors for D0$_{24}$ structure. But, for L1$_2$ structure, Young's modulus of Pd$_3$Ti is relatively higher than Pd$_3$Zr and Pd$_3$Hf.

The relations between the elastic moduli and the plastic properties of polycrystalline pure metals are proposed by Pugh [62]. It was stated that the Pugh's modulus ratio ($k=G/B$) represents a good criteria to identify the brittleness and ductility of materials [62]. In fact, it can be seen from [63] that Pugh's modulus ratio can be more correlated with hardness than the moduli of G and B, which only measures the elastic response. This is because Pugh's modulus ratio responds to both elasticity and plasticity, which are the most intrinsic features of hardness. In principles, the covalent materials have the highest hardness but they are obviously brittle with a larger Pugh's modulus ratio. On the contrary ductile materials with low Pugh's modulus ratio are characterized by metallic and/or ionic bonding and low hardness. According to the widely used semi-empirical Pugh's criterion (G/B ratio) [62], if $G/B<0.5$, a material will behave in a ductile manner and if $G/B>0.5$, a material demonstrates brittleness. In our case, the present values of the G/B are lower than 0.5 for these compounds, and hence, these materials will behave in a ductility manner.

Poisson's ratio can formally take values between −1 and 0.5, which corresponds, respectively, to the lower bound where the material does not change its shape and to the upper

Table 3 The calculated shear anisotropy factors (A_1, A_2, and A_3) for different planes and hardness (H_V in GPa) values for Pd$_3$X (X=Ti, Zr, Hf)

Material			A_1	A_2	A_3	H_V
Pd$_3$Ti (D0$_{24}$)	Present	(GGA)	0.72	0.72	1.00	10.92
Pd$_3$Ti (L1$_2$)	Present	(GGA)	1.32	1.32	1.32	10.75
Pd$_3$Zr (D0$_{24}$)	Present	(GGA)	0.74	0.74	1.00	10.61
Pd$_3$Zr (L1$_2$)	Present	(GGA)	1.47	1.47	1.47	6.62
Pd$_3$Hf (D0$_{24}$)	Present	(GGA)	0.73	0.73	1.00	10.65
Pd$_3$Hf (L1$_2$)	Present	(GGA)	1.48	1.48	1.48	6.75
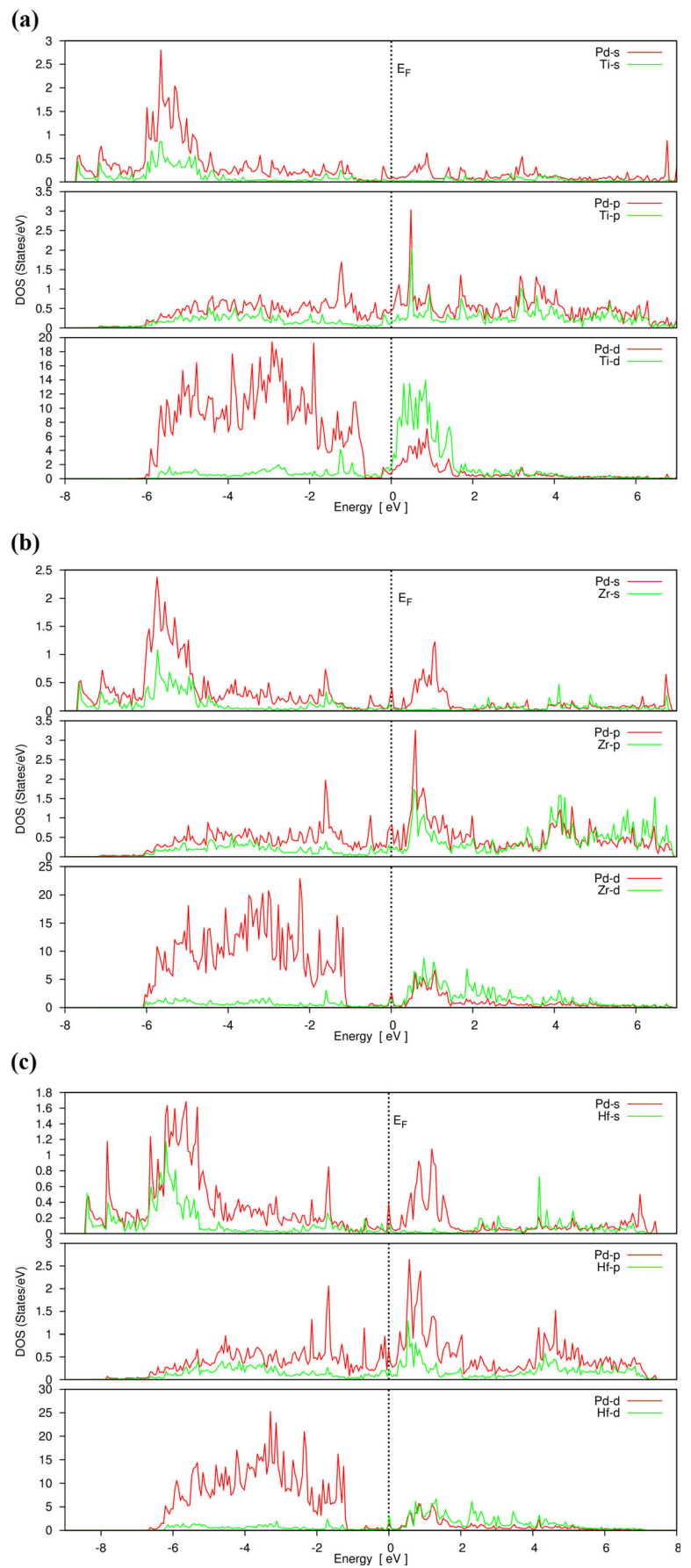
bound when the volume remains unchanged [64]. The value of Poisson's ratio is small (ν=0.1) for covalent materials, whereas for ionic materials, it has a typical value of ν=0.25 [62]. Our ν values are 0.29, 0.29, and 0.30 for $D0_{24}$ structure and 0.29, 0.33, and 0.34 for $L1_2$ structure of Pd_3X (X=Ti, Zr, Hf), respectively. Therefore, we can say that the ionic contributions to the atomic bonding are rather high for these compounds. Among the investigated compounds, Poisson's ratio of cubic Pd_3Hf is higher than Pd_3Ti and Pd_3Zr, indicating that Pd-Hf bonding is less directional.

The Zener anisotropy factor (A) is an indicator of the degree of anisotropy in the solid structure. The elastic anisotropy of crystal reflects bonding character in different directions and has an important implication since it correlates with the possibility to induce micro-cracks in materials [65]. For a completely isotropic material, the A_1, A_2, and A_3 factors take the value of 1; generally, it is known that when the value of A is smaller or greater than unity, it is a measure of the degree of elastic anisotropy. We have estimated the elastic shear anisotropy for investigated materials using the anisotropy factor [66] defined as: $A = A_1 = A_2 = A_3 = \frac{2C_{44}}{C_{11}-C_{12}}$ for cubic phases and $A_1 = A_2 = \frac{2C_{66}}{C_{11}-C_{13}}$ for the {1 0 0}({0 1 0}) shear planes between <0 1 1>(<1 0 1>) and <010>(<001>) directions, $A_3 = \frac{4C_{66}}{C_{11}+C_{22}-2C_{12}}$ for the {0 0 1} shear planes between <1 1 0> and <0 1 0> directions for hexagonal phases, and they are tabulated in Table 3 for $D0_{24}$ structure. The value of A_3 for each compound is equal to 1, indicating that {001} shear plane exhibits isotropy. On the contrary, for {100} and {010} shear planes, A_1 and A_2 are far from 1. Also, the anisotropy factors for $L1_2$ structure are far from 1 and the Pd_3Hf possesses larger anisotropy than others.

We have also calculated the hardness (H_V) of Pd_3X (X=Ti, Zr, Hf) by using a semi-empirical method based on Pugh's modulus (G/B) ratio developed by Chen et al. [63]. It is given as:

$$H_V = Ck^m G^n; \; (k = G/B) \qquad (4)$$

where the parameter k is the Pugh's modulus ratio. C is a proportional coefficient, and m and n are constants. In our case, the constants are: C=1.887, m=1.171, and n=0.591. The calculated hardness (H_V) values are also listed in Table 3. As shown in Table 3, in both $D0_{24}$ and $L1_2$ structures, Pd_3Ti has the highest hardness (10.92 and 10.75 GPa), while Pd_3Zr has the lowest (10.61 and 6.62 GPa). Actually, the calculated hardness values for all of Pd_3X (X=Ti, Zr, Hf) are under the superhardness limit ($H_V \geq 40$ GPa), indicating that these compounds except for Pd_3Zr and Pd_3Hf in $L1_2$ structure are relatively hard materials. Among the investigated Pd_3X compounds, Pd_3Ti has the largest G/B ratio which suggests the strongest directional bonding between Pd and Ti indicating

important effect on its hardness. Indeed, the estimated H_V for Pd_3Ti is largest one among the studied compounds.

3.3 Electronic Properties

We have calculated partial density of sates (PDOS) at zero pressure to understand the electronic nature of Pd_3X (X=Ti, Zr, Hf) compounds as shown in Fig. 1, where the vertical lines refer to the Fermi level. The PDOS of Pd_3X (X=Ti, Zr, Hf) exhibits non-zero values at Fermi level, which indicates the metallic feature of Pd_3X (X=Ti, Zr, Hf) compounds. The delocalized bands in the energy range between −8 and 0 eV is essentially dominated by Pd-d states, with a minor presence X-d. The partial DOS (PDOS) curves of Pd_3X reveal that Pd and X s-p orbital overlap over the energy range from −8 to 7 eV, which are evidently indicative of the covalent interactions between the Pd and X resulting from the strong hybridization. We can also see from Fig 1b, c that Fermi level of the Pd_3Zr and Pd_3Hf is located right in the deep valley and this so-called pseudo-gap. The present results are in accordance with the earlier reports on the study of [43]. For Pd_3Ti, peak in the conduction band mainly originates from the contribution of the Ti-d states but also contains a small Pd-d component, while for Pd_3Hf and Pd_3Zr, peak in the conduction band originates from Pd-d and Zr and Hf-d states nearly equally.

To further comprehend the bonding mechanism of Pd_3X (X=Ti, Zr, Hf) compounds, we have calculated the charge density distribution in (110) plane as shown in Fig. 2. Since these plots are very similar for Pd_3X (X=Ti, Zr, Hf), we have given only for Pd_3Ti. From Fig. 2, we have noticed that the charge density is essentially spherical around the atoms, with small covalent features. The charge density distribution maps between Pd and X atoms exhibit mainly ionic bonding with somewhat covalent bonding. A plot of charge densities clearly shows a net charge transfer from Pd to X, because X is more electronegative than Pd. Obtained results for charge densities for Pd_3X are in good agreement with the above-investigated PDOS curves and Poisson's ratio values.
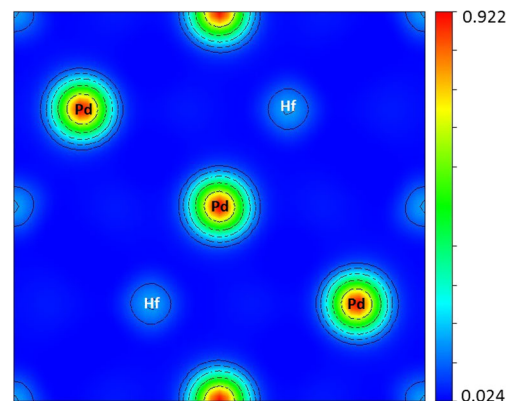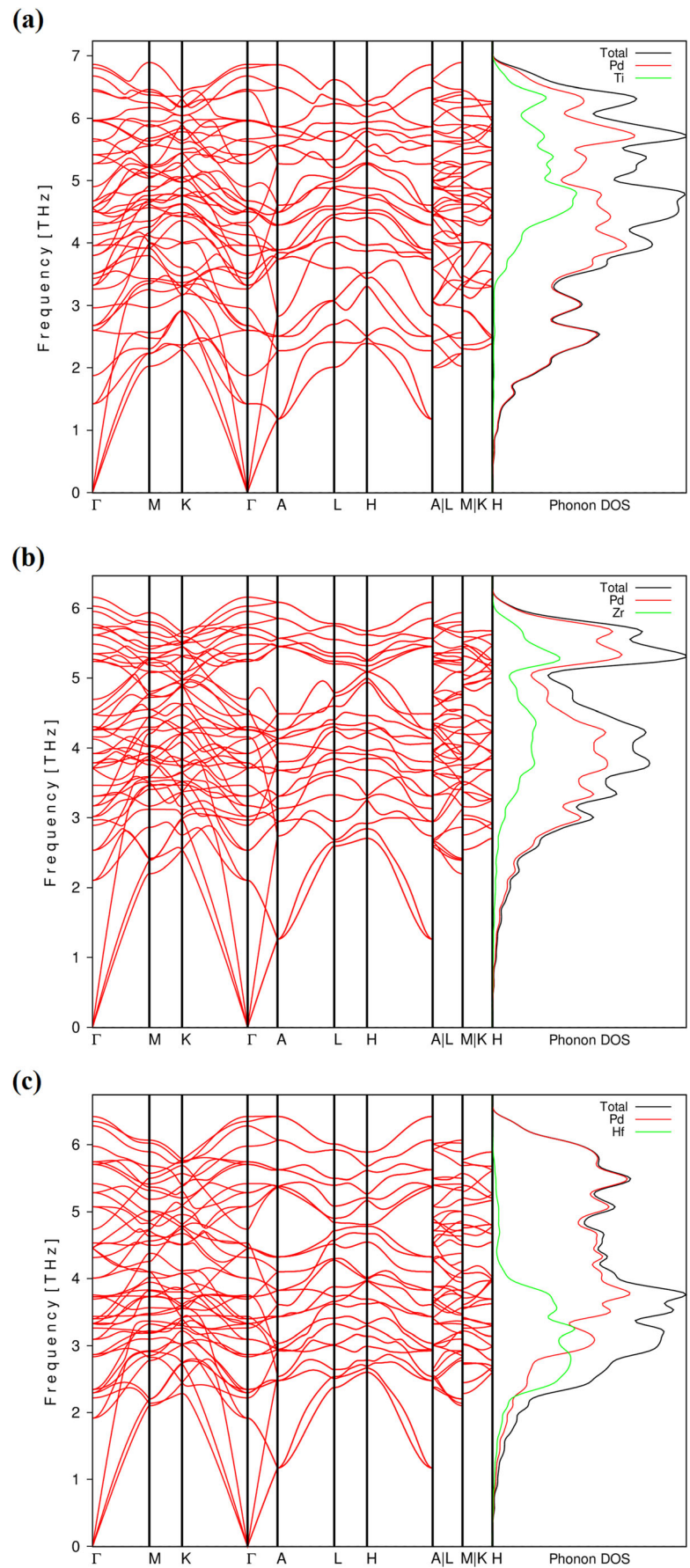

Fig. 2 The 2D charge density map in (110) plane for Pd_3Ti alloy (for similarity and simplicity, the others are not given)

Fig. 3 The phonon dispersions and corresponding phonon density of states for **a** Pd$_3$Ti, **b** Pd$_3$Zr, and **c** Pd$_3$Hf alloys

3.4 Lattice Dynamical Properties

The calculations show that the structural stability also depends on lattice dynamic properties. So, we also calculate lattice dynamical properties of Pd_3X. The present phonon frequencies in $D0_{24}$ phase are calculated by the PHONOPY code [67] using the interatomic force constants obtained from the VASP5.2. The PHONOPY code, based on real space of super-cell, calculates the force constant matrices and phonon frequencies using the "linear response method" within the density functional perturbation theory (DFPT) [67–70]. Specifically, the phonon dispersion curves in high symmetry directions and one-phonon density of state have been calculated using a $2\times2\times2$ super-cell approach. The obtained phonon dispersion curves and related one-phonon density of state along the high symmetry directions are illustrated in Fig. 3 for Pd_3X (X=Ti, Zr, Hf). Unfortunately, there are no experimental or other theoretical results on the lattice dynamics of these compounds from literature to compare with the present data.

It is seen from Fig. 3 that Pd_3X (X=Ti, Zr, Hf) have very similar dispersion curves and the corresponding density of states. The calculated phonon dispersion curves do not contain soft mode at any wave vectors, which confirms dynamically the stability of Pd_3X (X=Ti, Zr, Hf) in $D0_{24}$ structure. Therefore, we can expect that the optimized geometry of the Pd_3X lies at least in its local minimum energy. The unit cell of Pd_3X has 16 atoms, which give rise to a total of 48 phonon branches with three acoustic modes and 45 optical modes. For Pd_3X, a clear gap between optic and acoustic branches is not observed. It is well known that the mass difference between anions and cations strongly affects the maximum and minimum values of the acoustic and optic branches. Here, the maximum values of the phonon frequencies for optical branches decrease when going from Ti to Zr atom. It can be seen from Fig. 3 that all phonon branches are dispersive throughout the Brillouin zone. The phonon density of states is an important dynamical property as its computation needs phonon frequencies in the entire Brillouin zone [71]. On the right side of phonon dispersion curves, the corresponding partial phonon density of phonon state is also plotted in Fig. 3. The sharp peaks in the phonon DOS correspond to the flat modes of the phonon dispersion curves belonging to both optical and acoustical branches. We have not presented the calculated phonon dispersion curves for $L1_2$ structure of Pd_3X which have positive phonon frequencies in the main symmetry directions so as to save space in the journal due to the obtained phonon graphs for $L1_2$ are more or less similar to that of $D0_{24}$ structure.

We also calculated some thermodynamic properties such as free energy, entropy, and heat capacity at constant volume for $D0_{24}$ structure of Pd_3X by using the expressions within the quasi-harmonic approximation as given in [72] (See Figs. 4, 5, and 6). To study the thermodynamic properties at constant volume, one has to look at the free energy, incorporating the effects of phonon. Helmoltz free energy contains static contribution to internal energy at volume V and vibrational free energy which comes from the phonon contribution. Elastic constants of solids are determined based on the second-order derivative of the free energy according to strain. The free energy and entropy curves exhibit the expected behavior at

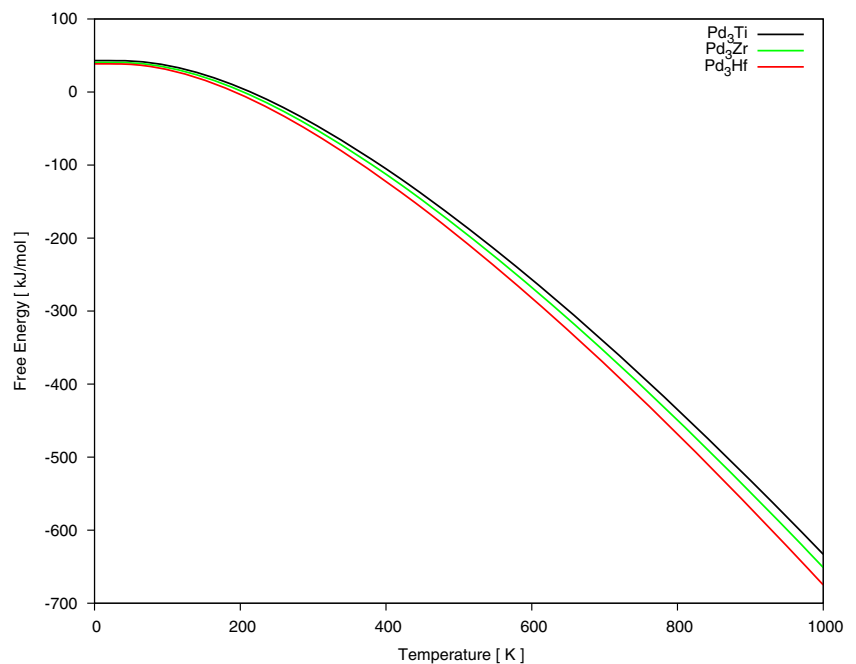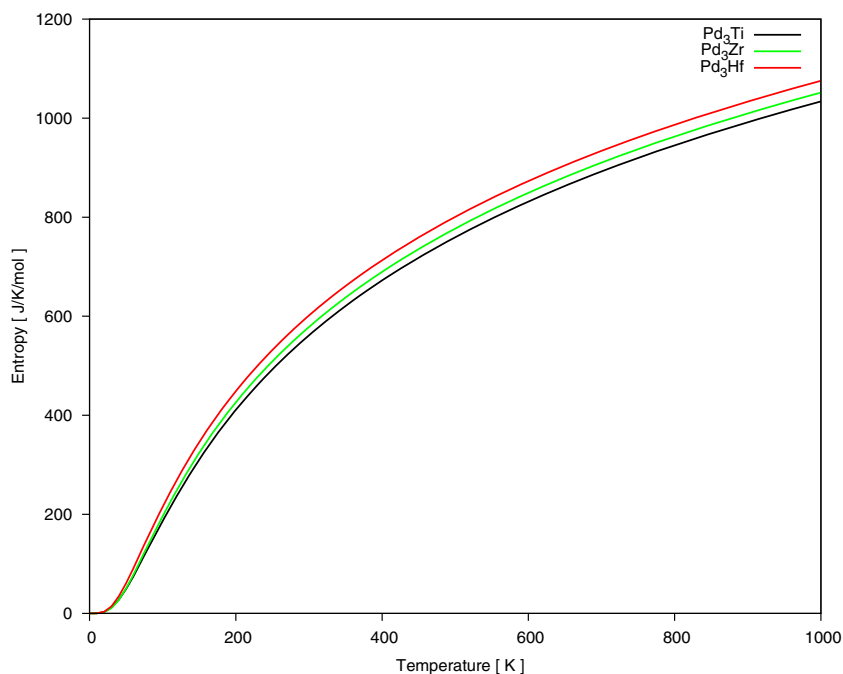**Fig. 4** The temperature dependence of free energy for Pd_3X (X=Ti, Zr, Hf) alloys

**Fig. 5** The temperature
dependence of entropy for Pd₃X
(X=Ti, Zr, Hf) alloys

the considered temperature range. While free energy decreases
with increasing temperature, the entropy increases. This be-
havior is due to the fact that both internal energy and entropy
increase with temperature, and hence it leads to the decrease in
free energy [73]. Also, the inspection of the free energy plots
suggests that examined compounds are thermodynamically
stable in the studied temperature range. The entropy variations
with the temperature are given at the same temperature range
in Fig. 5 for Pd₃X. Because of the vibrational contribution, the
entropy curves increase rapidly as temperature increases. The
increasing rate is relatively slower for Pd₃Ti compared to

Pd₃Hf and Pd₃Zr. These differences may be due to the higher
contribution of low phonon frequencies [63]. The contribution
to the total heat capacity from the lattice vibrations suggest
that while temperature is about $T<400$, heat capacity increases
very rapidly with temperature, however when the temperature
is about $T>400$, it increases slowly with the temperature. For
the present compounds, the heat capacity almost remains con-
stant at about 400 K and approaches the Dulong-Petit limit.
Unfortunately, there is no experimental or other theoretical
data on the lattice dynamical and thermodynamical properties
for these compounds for the sake of comparison.

Fig. 6 The temperature
dependence of heat capacity for
Pd₃X (X=Ti, Zr, Hf) alloys
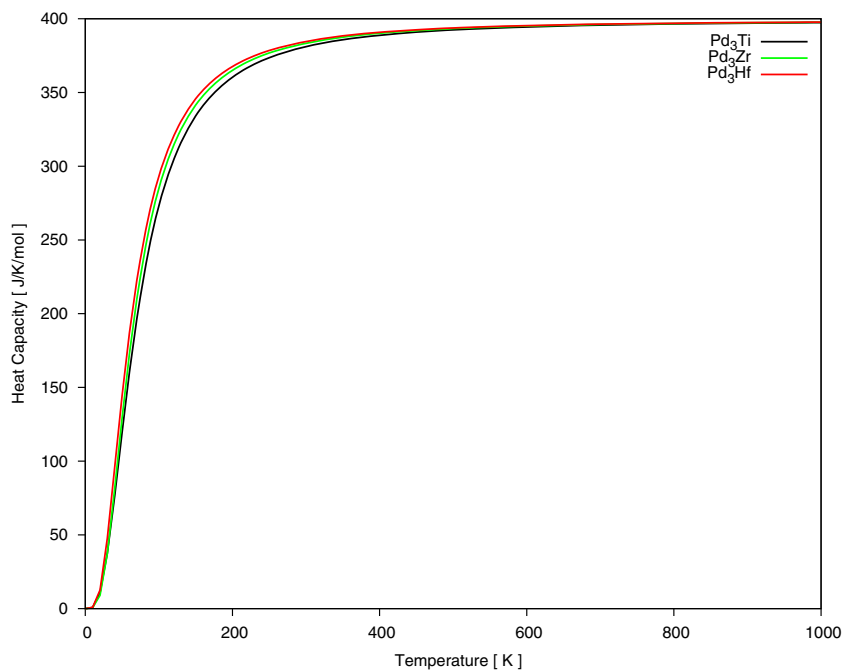
4 Summary and Conclusion

In this paper, the structural, mechanical, electronic, and lattice dynamical properties in the considered structures of Pd_3X (X=Ti, Zr, Hf) are presented using first-principle calculations. The obtained structural and elastic properties are in good agreement with available theoretical and experimental results. From the obtained elastic constants, we have analyzed its mechanical stability and some important physical quantities, such as bulk, Young's and shear moduli, G/B rations, and Poisson's ratios. Our results show that these compounds are mechanically stable and relatively hard materials with low compressibility. Phonon dispersion curves and density of states also confirm their dynamical stability in $D0_{24}$ structure. We have also computed and discussed the temperature-dependent thermodynamic properties such as free energy, entropy, and heat capacity in $D0_{24}$ structure. Finally, we can conclude that our results might serve as reliable predictions where the experimental data are lacking.

References

1. M. Ellner, J. Less-Common Met. **60**, 15 (1978)
2. M. Sundareswari, M. Rajagopalan, Eur. Phys. J. B **49**, 67–75 (2006)
3. Y. Terada, K. Ohkubo, S. Miura, J.M. Sanchez, T. Mohri, J. Alloys Compd. **354**, 202–207 (2003)
4. K. Chen, L.R. Zhao, J.S. Tse, J.R. Rodgers, Phys. Lett. A **331**, 400–403 (2004)
5. J.B. Moser, J.H.C. Lin, M. Taira, E.H. Greener, Dent. Mater. **1**, 37–40 (1985)
6. M. Nakagawa, S. Matsuya, Dent. Mater. J. **20**, 305–314 (2001)
7. M. Nishida, T. Hara, Y. Morizono, A. Ikeya, H. Kijima, A. Chiba, Acta Mater. **45**, 4847–4853 (1997)
8. K. Mizuuchi, K. Inoue, K. Yamauchi, K. Enami, M. Itami, Y. Okanda, Mater. Sci. Eng. A **316**, 93–101 (2001)
9. A. Kulińska, P. Wodniecki, Intermetallics **15**, 1190–1196 (2007)
10. R.C. Bowman Jr., A. Attalla, G.C. Abell, J.S. Cantrell, A.J. Maeland, J Less-Common Met. **172–174**, 643–651 (1991)
11. K. Yokoyama, T. Ogawa, K. Asaoka, J. Sakai, J Alloys Compounds. **400**, 227–233 (2005)
12. Z. Werner, J. Piekoszewski, A. Barcz, R. Grötzschel, F. Prokert, J. Stanislawski, W. Szymczyk, Nucl. Inst. Methods Phys. Res. B. **175–177**, 767–771 (2001)
13. J. Oak, A. Inoue, J. Non-Cryst, Solids **354**, 1828–1832 (2008)
14. M. Hwang, M. Meichle, M.B. Salamon, C.M. Wayman, Philos. Mag. **47A**, 9–30 (1983)
15. G.L. Zhao, T.C. Leung, B.N. Harmon, M. Keil, M. Mullner, W. Weber, Phys. Rev. B **40**, 7999–8001 (1989)
16. L.A. Bendersky, R.M. Waterstrat, J. Alloys Compd. **252**, L5 (1997)
17. N. Ohnishi, T. Onozuka, M. Hirabayashi, J. Mater. Sci. **26**, 2219–2228 (1991)
18. K. Cenzual, J.L. Jorda, E. Parthe, Acta Crystallogr. **C44**, 14–18 (1988)
19. K. Cenzual, E. Parthe, Acta Crystallogr. **C42**, 1101–1105 (1986)
20. L.A. Bendersky, J.K. Stalick, R.M. Waterstrat, J. Alloys Compd. **201**, 121–126 (1993)
21. S.F. Dubinen, A.I. Lotkov, S.G. Teploukhov, V.N. Grishkov, V.P. Skorobogatov, Phys. Met. Metallogr. **73**, 401–405 (1992)
22. B.H. Chen, H.F. Franzen, J Less-Common Met. **153**, L13–L19 (1989)
23. B.H. Chen, H.F. Franzen, J. Less-Common Met. **158**, L11 (1990)
24. R.M. Waterstrat, R. Kuentzler, J. Muller, J Less-Common Met. **167**, 169–178 (1990)
25. J.-Q. Hu, M. Xie, X. Pan, Y.-C. Yang, M- M. Liu, J.-M. Zhang. Comput. Mater. Sci. **51**, 1 (2012)
26. L. Brewer, Acta Metall. **15**, 553–556 (1967)
27. Q. Guo, O.J. Kleppa, J. Alloys Compd. **266**, 224 (1998)
28. M. Ellner, J. Alloys Compd. **366**, 222 (2004)
29. E. Raub, E. Röschel, Z. Metallk. **59** (1968) 112
30. I.R. Harris, M. Norman, J. Less Common Met. **22**, 127 (1970)
31. H. Schulz, K. Ritapal, W. Bronger, W.Z. Klemm, Anorg Allg Chem **357**, 299 (1968)
32. N. Selhaoui, J.C. Gachon, J. Hertz, J Less Common Met. **154**, 137 (1989)
33. S. Curtarolo, D. Morgan, G. Ceder, Comput Coupling of Phase Diagrams and Thermochem. **29**, 163–211 (2005)
34. P. Villars, K. Cenzual, J.L. Daams, F. Hulliger, H. Okamoto, K. Osaki, A. Prince, Pauling File, Binaries ed., Inorganic Materials Database and Design System, Version 1.0, distributed by Crystal Impact, 2001.
35. R.F. Minibaev, D.I. Bazhanov, A.A. Katsnel'son, S.E. Kul'kova, D.S. Xu, Q.M. Hu, Y.L. Hao, Journal of Surface Investigation. X-ray, Synchrotron and Neutron Techniques 1 (2007) 754.
36. P. Mikusik, S. Pick, Solid State Commun. **86**, 467 (1993)
37. S. Pick, P. Mikusik, Solid State Commun. **80**(10), 897 (1991)
38. C. Guo, Z. Du, C. Li, Calphad **30**, 482 (2006)
39. Q. Guo, O.J. Kleppa, J. Alloys Compd. **266**, 224 (1998)
40. X.Q. Chen, C.L. Fu, J.R. Morris, Intermetallics **18**, 998 (2010)
41. S.V. Meschel, P. Nash, X.Q. Chen, J. Alloys Compd. **492**, 105 (2010)
42. X. Bai, J.H. Li, Y. Dai, B.X. Liu, Intermetallics **31**, 79 (2012)
43. G. Surucu, K. Colakoglu, E. Deligoz, N. Korozlu, H. Ozisik, Comput. Mater. Sci. **48**, 859–865 (2010)
44. G. Surucu, K. Colakoglu, E. Deligoz, H. Ozisik, Intermetallics **18**, 286 (2010)
45. G. Kresse, J. Hafner, Phys. Rev. B **47**, 558 (1994)
46. G. Kresse, J. Furthmüller, Comput. Mater. Sci. **6**, 15 (1996)
47. G. Kresse, D. Joubert, Phys. Rev. B **59**, 1758 (1999)
48. G. Kresse, J. Furthmüller, Phys. Rev. B **54**, 11169 (1996)
49. P.E. Blochl, Phys. Rev. B **50**, 17953 (1994)
50. J.P. Perdew, K. Burke, M. Ernzerhof, Phys. Rev. Lett. **77**, 3865 (1996)
51. H. Monkhorst, J. Pack, Phys. Rev. B **13**, 5188 (1976)
52. U.V. Choudary, K.A. Gingerich, L.R. Cornwell, Metall Trans **8A**, 1487 (1977)
53. A.E. Dwight, P.A. Beck, Trans. Metall. Soc. AIME **215**, 976 (1959)
54. A.F. Jankowski, J. Alloys Compd. **182**, 35 (1992)
55. V. Kanchana, G. Vaitheeswaran, A. Svane, A. Delin, J. Phys. Condens. Matter **18**, 9615 (2006)
56. Y.L. Page, P. Saxe, Phys. Rev. B **65**, 104104 (2002)
57. D.C. Wallace, *Thermodynamics of crystals* (Wiley, New York, 1972)
58. M. A. Baranov, E.A. Dubov, EPhTJ 1 (2005) 28
59. B. Mayer, H. Anton, E. Bott, M. Methfessel, J. Sticht, P.C. Schmidt, Intermetallics **11**, 23 (2003)
60. A.A. Maradudin, E.W. Montroll, G.H. Weiss, I.P. Ipatova, *Theory of Lattice Dynamics in the Harmonic Approximation*, 2nd edn. (Academic, NewYork, 1971)
61. K. Chen, L.R. Zhao, J. Rodgers, J.S. Tse, J. Phys. D. Appl. Phys. **36**, 2725 (2003). doi:10.1088/0022-3727/36/21/021
62. S.F. Pugh, Philos. Mag. **45**, 823 (1953)
63. X.Q. Chen, H. Niu, D. Li, Y. Li, Intermetallics **19**, 1275 (2011)

64. S.G. Said, H. Ozisik, E. Deligoz, M.B. Kanouni, Semicond. Sci. Technol. **28**, 085005 (2013)
65. P. Ravindran, L. Fast, P.A. Korzhavyi, B. Johansson, J. Wills, O. Eriksson, J. Appl. Phys. **84**, 4891 (1998)
66. N. Miao, B. Sa, J. Zhou, Z. Sun, Comput. Mater. Sci. **50**, 1559 (2011)
67. A. Toga, F. Oba, I. Tanaka, Phys. Rev. B **78**, 134106 (2008)
68. S. Baroni, P. Giannozzi, A. Testa, Phys. Rev. Lett. **58**, 1861 (1987)
69. X. Gonze, J.-P. Vignenon, Phys. Rev. B **39**, 13120 (1989)
70. X. Gonze, D.C. Allan, M.P. Teter, Phys. Rev. Lett. **68**, 3603 (1992)
71. P.K. Jha, Phys. Rev. B **72**, 214502 (2005)
72. R. Wang, S. Wang, X. Wu, T. Song, Int. J. Thermophys. **33**, 300 (2012)
73. K.R. Babu, C.B. Lingam, S. Auluck, S. Tewari, G. Vaitheeswaran, J. Solid Chem. **184**, 343 (2011)